Invited paper

Fluorescence interference-contrast microscopy of cell adhesion on oxidized silicon

D. Braun, P. Fromherz*

Department of Membrane and Neurophysics, Max-Planck-Institute for Biochemistry, D-82152 Martinsried-München, Germany
(Fax: +49-89/8578-2822, E-mail: fromherz@biochem.mpg.de)

Abstract. Standing modes of light in front of the reflecting surface of silicon modulate the excitation and emission of fluorescent dyes. This effect was used to determine the distance of a biomembrane from an oxidized silicon chip. The membrane of a red blood cell (ghost) was stained with a cyanine dye and attached with poly-lysine to a surface structured with microscopic steps of silicon dioxide on silicon. The system was illuminated in a microscope. The fluorescence intensity of the membrane depended on the height of the steps. The data were fitted by an optical theory which accounts both for the interference of the exciting light and for the interference of the emitted light at a finite aperture. The distance between the membrane and the silicon dioxide was determined to be 12 nm.

PACS: 33.50.D; 68.35.G; 78.66; 87.22

Nerve cells and silicon devices can be joined by electrical induction when the cell membrane is attached closely to an oxidized chip [1]. Recording as well as stimulation of neuronal activity from oxidized silicon have been reported [2, 3]. The strength of coupling depends on the width of the electrolyte which separates the insulating layers of the cell membrane and the silicon dioxide. This width was estimated to be in the range 10–100 nm on the basis of the coupling experiments themselves [4]. No direct measurements are available.

Usually the attachment of cells to surfaces is studied by reflection interference contrast microscopy (IRM/RICM) [5–9] or by total internal reflection fluorescence microscopy (TIRFM) [10–15]. In both methods the cell is illuminated by visible light through a transparent support. In the RICM method the light is reflected from the substrate/electrolyte and electrolyte/cell interfaces and gives rise to an interference pattern. In the TIRFM method the cell is illuminated under the condition of total reflection; the membrane or electrolyte are labelled with a fluorescent dye which is excited by the evanescent wave.

RIC-microscopy and TIRF-microscopy cannot be used for cells on silicon, which is not transparent in the visible range. For that reason a new method of fluorescence interference contrast (FLIC) microscopy was proposed to map the distance between a membrane and oxidized silicon [16]. FLIC-microscopy takes advantage of the Wiener effect [17–19], the interference of incident and reflected light above a mirror. The standing modes of the electromagnetic field above the surface of silicon modulate the excitation and the emission of a fluorescent dye which is dispersed in an adjacent solvent or bound to a macromolecule or membrane. Some features of FLIC-microscopy were tested with a dry monomolecular film [16].

In this paper we consider FLIC-microscopy as a tool to study cell adhesion. It is applied to determine the distance between a biomembrane and a silicon chip. As a test system we used ghosts of human erythrocytes because of their homogeneous membrane. In the first part we describe the concept of the method and explain the experimental technique. In the second part we present the data and discuss the results.

1 Materials and methods

First we consider the principles of FLIC-microscopy as applied to cell adhesion. Then we describe the fabrication of the chips, the preparation of stained erythrocyte membranes, the attachment of the cells to the chip, the photometric set-up, the optical theory and the evaluation of the data.

1.1 Principles of FLIC-microscopy

Silicon reflects visible light. The interference of the incident light with the reflected light gives rise to standing modes of the electromagnetic field. As a result the electronic excitation of a dye molecule depends on its position in front of the mirror. By analogy, the fluorescence emission of a dye molecule is affected due to the interference of light which is emitted with and without reflection, or in other words due to emission into an unoccupied standing mode of the electromagnetic field.
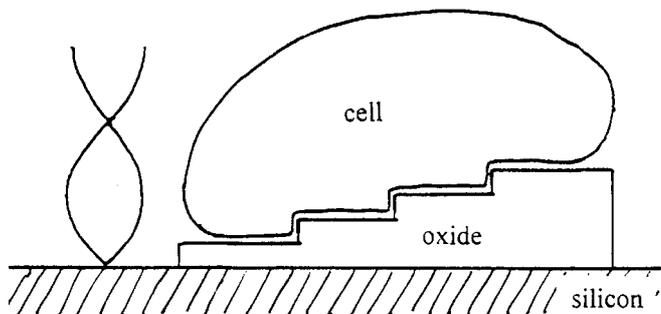
---

*Correspondence author

Fig. 1. Fluorescence interferometry of cell adhesion. A cell is attached to microscopic steps (height $\sim 50\,\text{nm}$, width $\sim 5\,\mu\text{m}$) of silicon dioxide on silicon. The extracellular surface of the membrane is stained with an amphiphilic fluorescent dye. The fluorescence intensity depends on the position of the dye with respect to the standing modes of light in front of the reflecting surface of silicon, i.e. on the variable height d_{ox} of the steps and on the constant distance d_{cleft} between oxide and membrane

We consider a cell membrane which is labelled at its extracellular surface by a fluorescent dye. The cell is attached to silicon covered with a thin film of silicon dioxide as illustrated in Fig. 1. We use different heights of the oxide beneath a single cell. The fluorescence intensity depends on the thickness d_{ox} of the oxide and on the distance d_{cleft} between oxide and membrane. d_{cleft} is determined by the local forces between membrane and oxide. A changed width d_{ox} of the spacer brings the membrane to a different position in the electromagnetic field at constant d_{cleft}. We expect a periodic modulation of the fluorescence intensity $J_{fl}(d_{ox})$ with increasing thickness d_{ox}. The phase of that modulation depends on the increment d_{cleft}. If we know the theoretical relation $J_{fl}(d_{ox}, d_{cleft})$ of the fluorescence intensity, we can fit the data with the unknown separation d_{cleft} as a free parameter.

1.2 Ghosts

We prepared the membranes of human erythrocytes according to a standard procedure [20] with some minor modifications. 4 ml of blood from healthy colleagues were sucked into a tube coated with EDTA to prevent coagulation (Vacutainer 367861, Becton Dickinson, Meylan, France). The blood was centrifuged for 10 min at 1600 g. The pellet (1.5 ml) was collected in a pipette. We washed the erythrocytes three times by resuspension and centrifugation for 10 min at 1600 g using 20 ml of a 300 mOsm TRIS buffer (6.05 g TRIS, 6.42 g NaCl, 420 ml 0.1 M HCl, 580 ml Milli-Q water (Millipore), pH 7.4). 1.5 ml of the final pellet were diluted with 1.5 ml TRIS buffer and kept for several hours at 4 °C.

Transient lysis of the erythrocytes was performed on ice with precooled solutions. At first we added 15 ml of a 30 mOsm lysing solution (301 mg MgSO₄, 372 mg KCl in 500 ml Milli-Q water) to 0.5 ml of the cell suspension. Immediately afterwards 1 ml of a resealing solution (53.7 g KCl, 10.5 g NaCl in 400 ml Milli-Q water) was added. The suspension was kept for 5 min on ice and for 30 min at 37 °C. The ghosts were centrifuged for 10 min at 3000 g.

1.3 Staining

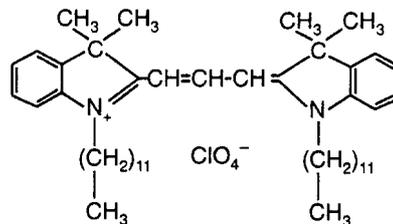We stained the ghost membrane with a homolog of the amphiphilic trimethin-indocarbocyanine dye S27/DiIC$_{18}$ [18,

Fig. 2. Amphiphilic trimethin-indocarbocyanine dye DiIC$_{12}$ used to stain the erythrocyte membrane

21–23] with two dodecyl-chains (DiIC$_{12}$, Molecular Probes) (Fig. 2). Three aspects were relevant for the choice of this dye: (i) The transition dipole of excitation and emission is parallel to the cell membrane [24]; (ii) the flip-flop of the dye from one side of the membrane to the other side is slow [25]; (iii) photobleaching of the dye is rather weak [26].

We made a 5 mM solution of the dye in ethanol. 5 μl were added to 15 ml TRIS buffer such that a suspension of microcrystals was formed. It was used to resuspend the upper (liquid) part of the centrifuged pellet of ghosts. We isolated the stained ghosts immediately afterwards by centrifugation at 3000 g for 10 min. The supernatant with the microcrystals of the dye were discarded and the ghosts were resuspended in 15 ml TRIS buffer. Most ghosts had an erythrocyte-like shape. Some were spherical with a diameter of about 6 μm.

1.4 Chips

We prepared chips from polished n-doped (4–8 Ωcm) four-inch silicon wafers (Freiberger, Freiberg, Germany). They were cleaned by the standard RCA procedure [27]. We prepared a homogeneous layer of silicon dioxide with a thickness of about 135 nm by thermal growth in an oven at 1000 °C (E1200 Lab, Centrotherm, Blaubeuren). The wafer was covered with a photoresist by spin-coating and illuminated in a mask-aligner through a metal mask with stripes of 5 μm width, separated by 5 μm. After development we removed about 83 nm of the oxide in the open areas by etching with fluoric acid [27]. Then the photoresist was stripped, the wafer was cleaned and coated again with photoresist. In a second illumination we used the same mask rotated by 90 °. After development we removed about 42 nm of the oxide in the open areas. Then the photoresist was stripped and the wafer was cut into chips (3.4 cm × 1.0 cm). The surface exhibited a pattern of squares with 5 μm edge length as illustrated in Fig. 3. The heights of the oxide were about 11, 53, 92 and 135 nm.
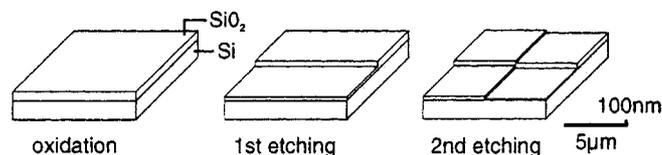

Fig. 3. Fabrication of chip. A homogeneous layer of thermal oxide with a thickness $\sim 130\,\text{nm}$ is grown on silicon. A step is etched down to an oxide thickness $\sim 50\,\text{nm}$. Two further levels with heights $\sim 90\,\text{nm}$ and $\sim 10\,\text{nm}$ are obtained by etching a step in the perpendicular orientation. Using a periodic mask, the surface of the chip is modulated by a periodic pattern of steps with a lattice constant of 10 μm. Note that the height of the steps is scaled by a factor of five

The chips were sonicated for 10 min at 70 °C in an acidic detergent (5% Ultrax 102, KLN Heppenheim), rinsed with Milli-Q water (Millipore Inc.), sonicated for 2 min at 70 °C in an alkaline detergent (2% Tickopur RP100, Bandelin, Berlin) and rinsed with Milli-Q again. Then the chips were sonicated four times in Milli-Q water for 10 min (twice at 70 °C, twice at room temperature) and dried with nitrogen [16, 28]. After cleaning, the thickness of the oxides was measured by an ellipsometer (SD 2000, Plasmos, München) using a refractive index $n_{ox} = 1.460$ at 633 nm. For that purpose we used a quadruple of reference squares with a size 500 μm × 500 μm which were arranged on the chip at a separation of 1 cm. They were fabricated together with the microscopic steps under identical conditions of etching.

1.5 Adhesion

The chips were placed into a petri dish of 35 mm diameter (Falcon 3001, Becton Dickinson, Plymouth). The ghost membrane did not adhere to clean silicon dioxide as it is negatively charged [29]. We used poly-lysine to induce attachment [30]. The chips were incubated in a solution of poly-L-lysine (MW 10,000, Sigma, Heidelberg) in TRIS buffer at a concentration of 0.5 mg/ml for 2 h at room temperature. They were rinsed three times with TRIS buffer. (The layer of poly-L-lysine had a thickness of about 0.7 nm after rinsing with milli-Q water and drying, as estimated by ellipsometry.) 3 ml of the suspension of ghosts were added to the wet chip. The ghosts were allowed to sediment for 20 min. We removed the liquid with non-adhering cells carefully and added 3 ml of TRIS buffer.

1.6 Photometry

The fluorescent ghosts were studied in the same set-up as used for monomolecular films [16]. A water immersion objective (100×) with a numerical aperture 1.0 was used in the microscope (Axioskop, Zeiss, Oberkochen). The cells were focused in red light (> 630 nm). Then the chip was illuminated monochromatically at 546 nm by a high pressure mercury lamp (Zeiss) through a dichroic mirror (Q565LP, AHF Analysentechnik, Tübingen) and a bandpass filter (546/10 nm, 546FGS, Andover, Salem, NH, USA). The fluorescence was detected around 610 nm through the dichroic mirror and a bandpass filter (610/70 nm, AHF Analysentechnik, Tübingen).

A fluorescence picture was taken by illumination for 40 ms. We used a CCD camera with 752 × 582 pixels (Sony chip ICX039AL, HRX, Theta System, München). The size of a single pixel corresponded to approximately 90 nm × 90 nm of the object. The signal of every second line of the camera was transferred to a PC by a frame grabber (ITEX AFG, Stemmer, München) with 8-bit resolution. We evaluated the stored fluorescence pictures in three steps: (i) the adhesion area of a single ghost was approximated by an ellipse and divided into four sectors on each oxide step; (ii) the number of pixels with a certain brightness was counted on each sector to form four histograms of the intensities; (iii) Gaussians were fitted to the histograms. The lowest components (< 10%) of a histogram were not considered.

1.7 Theory

The fluorescence intensities (average with standard deviation) on the four oxides of different thickness were fitted by an optical theory of interference. We summarize here the crucial relations. For details see [16, 31].

The probability per unit time P_{ex} for excitation of a dye molecule is determined by the intensity of illumination $I(\lambda_{in})$ (quanta per area, time and wavelength interval), the extinction coefficient of the dye $\varepsilon(\lambda_{in})$ and the relative strength F_{in} of the electrical field of incident light at the position of the dye projected onto the direction e_{ex} of the transition dipole of excitation. We obtain (1) by averaging over all directions and polarizations of the incident light within the aperture of the microscope, by averaging over all orientations of the dye in the plane of the membrane and by integration over all wavelengths λ_{in} of the incident light[1]:

$$P_{ex} \propto \int d\lambda_{in} I(\lambda_{in}) \varepsilon(\lambda_{in}) \langle |F_{in} \cdot e_{ex}|^2 \rangle \,. \tag{1}$$

The probability per unit time P_{em} to detect an emitted quantum from an excited molecule is given by (2) below. It depends on the quantum yield $\Phi_{det}(\lambda_{out})$ of the detection system, on the fluorescence spectrum (quanta per wavelength interval) of the dye, on the relative strength F_{out} of the local electrical field of that mode which accepts the emitted photon and on the direction e_{em} of the transition dipole of emission. We average over the polarizations and directions of detected light within the aperture of the microscope and over the orientations of the dye in the plane of the membrane. Finally we integrate over the wavelengths of detection λ_{out}:

$$P_{em} \propto \int d\lambda_{out} \Phi_{det}(\lambda_{out}) f(\lambda_{out}) \langle |F_{out} \cdot e_{em}|^2 \rangle \,. \tag{2}$$

The local relative field strengths F_{in} and F_{out} depend on the optical properties of the assembly and on the position of the dye molecule, in particular on the thickness d_{ox} of the oxide and on the distance d_{cleft} between membrane and support. They are computed by matrix methods [16, 32].

Under stationary illumination we detect an average flow J_{fl} of quanta per unit time from a dye molecule. It depends on the probability of detected quanta per unit time P_{em} from an excited molecule and on the probability that the molecule

[1]The various directions of exciting radiation may be integrated in the membrane (medium 3) at the position of the absorbing dye and the directions of emitted radiation in water (medium 4) at the entrance of the detecting objective. The energy flows per unit polar angle $d\Theta_3^{in}$ and $d\Theta_4^{out}$, respectively, depend on the direction, even if the illumination through the objective and the emission from the dye are homogeneous with respect to different directions within the angle of aperture. This effect is due to refraction and becomes important for high apertures as used in the present experiments. It can be described as a modulation of the intrinsic aperture functions – which are $A_{in}(\Theta_3^{in}) = 1$ and $A_{out}(\Theta_4^{out}) = 1$ within the angle of aperture and zero elsewhere – as $\left(\frac{n_3 \cos \Theta_3^{in}}{n_4 \cos \Theta_4^{in}}\right) A_{in}(\Theta_3^{in})$ and $\left(\frac{n_4 \cos \Theta_4^{out}}{n_3 \cos \Theta_3^{out}}\right) A_{out}(\Theta_4^{out})$, respectively, with Θ_4^{in} expressed by Θ_3^{in} and Θ_3^{out} by Θ_4^{out} according to Snellius' law. Appropriate substitutions are to be made when the integration of illumination is computed in water (medium 4), too.

is in its excited state. We obtain (3) with the total transition probabilities of fluorescence k_{fl} and of nonradiative decay k_{nr}:

$$J_{fl} = \frac{1}{k_{fl} + k_{nr}} \cdot P_{ex} \cdot P_{em} . \tag{3}$$

If the transition probabilities of fluorescence and nonradiative decay are independent of the thickness of the oxide, we may use (4). This approximation was shown to be adequate for the cyanine dyes S9 [16] and S27/DiIC$_{18}$ [31] in a dry monomolecular lipid film as well as in a wet lipid membrane:

$$J_{fl} \propto P_{ex} \cdot P_{em} . \tag{4}$$

1.8 Optical model

We describe the optics of an adhesion site by a model with five homogeneous and isotropic layers as sketched in Fig. 4. It consists of bulk silicon, a layer of silicon dioxide (thickness d_{ox}), a layer of the extracellular medium (thickness d_{cleft}), the cell membrane (thickness d_{mem}) and the intracellular medium. The complex refractive index of silicon (refractive index n_{Si}, attenuation index κ_{Si}) was taken from [33]. We used the table of refractive index of silica from [34] and matched the dispersion of the table to a refractive index $n_{ox} = 1.460$ at 632.8 nm of our thermally grown oxide. (The same value was used to determine the thickness of the oxide by ellipsometry.) We described the extracellular cleft by the refractive index of water $n_{cleft} = 1.333$. The membrane was characterized by a thickness $d_{mem} = 4$ nm [7] and a refractive index $n_{mem} = 1.450$ [7]. For the cytoplasm we used the refractive index of water $n_{cyt} = 1.333$. In the model the dye molecule was placed within the membrane layer close to its lower surface. The transition moments of excitation and emission were aligned parallel to the membrane with random orientation in the plane. The angles of aperture in water were 47.3° for excitation and 48.6° for emission. These values correspond to numerical apertures of 0.985 and 1.0 of the objective, respectively. The lower aperture for excitation was assigned on the basis of systematic measurements of fluorescence interference with supported lipid membranes [31]. The excitation was monochromatic with $\lambda_{in} = 546$ nm. An emission
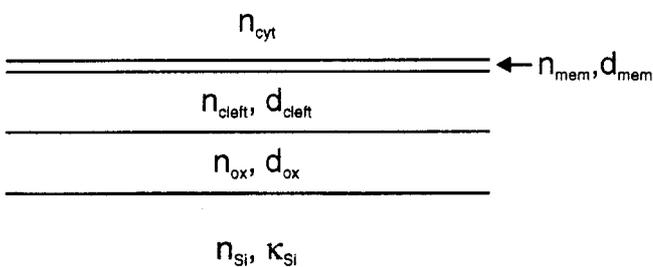
Fig. 4. Five-layer model of the optics of cell adhesion with bulk silicon (refractive index n_{Si}, attenuation index κ_{Si}), silicon dioxide (thickness d_{ox}, refractive index n_{ox}), extracellular medium (thickness d_{cleft}, refractive index n_{cleft}), membrane (thickness d_{mem}, refractive index n_{mem}) and cytoplasm (refractive index n_{cyt})

spectrum $f(\lambda_{out})$ was used as measured in a 1 μM ethanolic solution with a maximum at 565 nm. The spectrum of the quantum yield of detection $\Phi_{det}(\lambda_{out})$ was given by the data sheet of the camera and the transmission of the dichroic mirror and the optical filter.

Examples of theoretical relations $J_{fl}(d_{ox})$ are shown in Fig. 5 for three different distances $d_{cleft} = 0, 10, 20$ nm between membrane and oxide. The fluorescence intensity is very low close to the silicon. It increases and decreases with the thickness of the spacer. The phase of that modulation is shifted by an enhanced distance d_{cleft} between oxide and membrane.

1.9 Fit of data

We used three parameters to fit the theory to the experimental fluorescence intensities of the membrane on four oxides with defined thickness d_{ox}: (i) the unknown width d_{cleft} of the extracellular cleft; it affects mainly the phase of the wave $J_{fl}(d_{ox})$ of detected fluorescence; (ii) a scaling factor of the fluorescence intensity; it determines the amplitude of the wave of detected fluorescence; (iii) a constant increment which accounts for background fluorescence; it was mainly due to the upper side of the cell which was out of focus. From the data we calculated the values of the scaling factor and of the background analytically. Then we fitted d_{cleft} by the regression algorithm of Powell [35], adopting the estimate of the standard deviation of d_{cleft} from the Marquardt algorithm [35]. This evaluation presumes that the cell membrane is stained homogeneously and that no dye is adsorbed to the oxide.

2 Results and discussion

A photograph of fluorescent erythrocyte ghosts on a silicon chip is shown in Fig. 6. Four levels of fluorescence intensity are seen for each cell. They are due to the stained membrane attached to the four steps of silicon dioxide with different
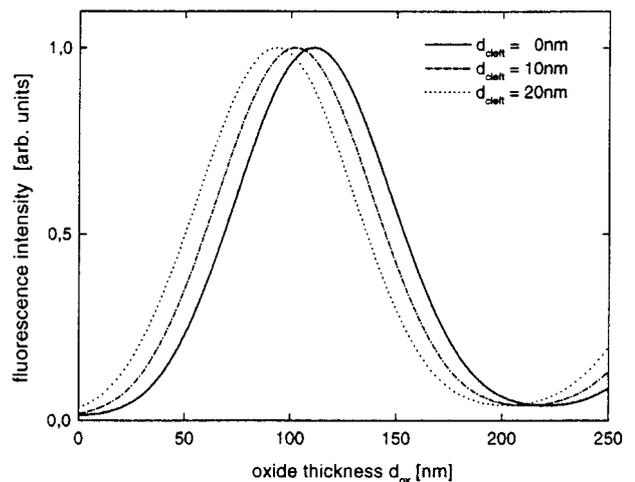
Fig. 5. Theory. Relative fluorescence intensity of the dye DiIC$_{12}$ in a cell membrane versus thickness d_{ox} of silicon dioxide for the distances $d_{cleft} = 0, 10, 20$ nm between membrane and silicon dioxide

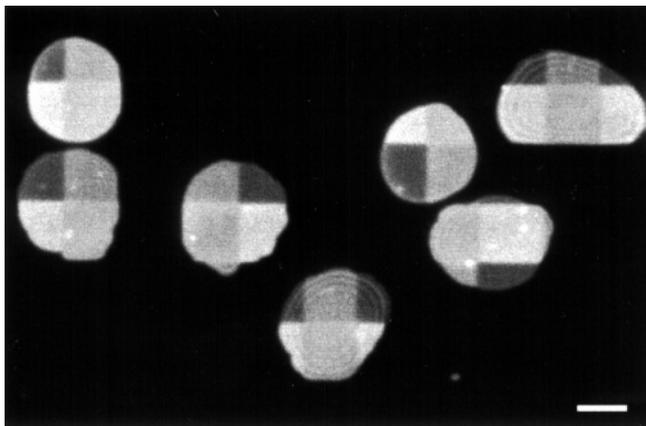**Fig. 6.** Photograph of fluorescent erythrocyte membranes (ghosts) stained with the dye $DiIC_{12}$ on stepped silicon dioxide on silicon. Four areas of homogeneous fluorescence are seen in each cell due to the membrane attached to four levels of oxide. In some cells this pattern is superposed by a sequence of rings. The scale bar is 5 µm

height. On each step the intensity is rather homogeneous. In some cells a ring-shaped pattern is superposed. It is due to the upper part of the cell when it has the shape of a flat cupola being within the focus of the microscope.

First we evaluate the fluorescence intensities of the attached membrane of one selected cell. Then we consider a population of attached ghosts. Finally we evaluate the profile of the upper membrane from the ring-shaped pattern.

2.1 Single cell

A digitized image of a selected cell is depicted in Fig. 7. The height of the steps of silicon dioxide is indicated. The fluorescence is low on the thinnest oxide of 10.9 nm, modest on the oxide of 52.7 nm, bright on the oxide of 92.1 nm and modest again on the oxide of 135.4 nm. The histograms of the intensities within the four areas are shown in the figure. The data were fitted by Gaussians. The average intensities and the width of the distributions ($\pm\sigma$) are plotted versus the height of the steps in Fig. 8.

The four data points in Fig. 8 were fitted with the optical theory of interference using (4) with (2) and (3). The wavelength of excitation, the spectrum of emission, the sensitivity spectrum of detection and the apertures of excitation and emission were defined by the optical set-up. They determine the period of the wave. The five-layer model (Fig. 4) with silicon, silicon dioxide, extracellular medium, membrane and intracellular medium determined the phase of the wave. The distance d_{cleft} of the outer surface of the membrane from the silicon dioxide was a free parameter. The other free parameters were the amplitude of the wave and a constant background. As a result we obtained $d_{\text{cleft}} = 12.1$ nm.

2.2 Accuracy

The total statistical errror of the distance d_{cleft} of a single ghost had two sources: the error of the fit of the optical theory and the uncertainty of the thickness of the oxides. We found that the statistical deviation of the fit was $\Delta d_{\text{cleft}} = \pm 0.4$ nm.

The second error was due to the different positions of ellipsometry and ghost on the chip. The uncertainty of the oxide thickness within 1 cm along the chip was ± 0.1 nm. Thus the total statistical error of the distance between membrane and oxide was $\Delta d_{\text{cleft}} = \pm 0.41$ nm.

There were three sources of systematic errors: (i) the measurement of thickness by the ellipsometer; (ii) the measurement of fluorescence intensity by the CCD camera and by digitization; and (iii) the uncertainty of the parameters which enter the optical model. We estimated the precision of the ellipsometer to be $\Delta d_{\text{ox}} = \pm 0.2$ nm. This corresponds to an error of $d_{\text{cleft}} = \pm 0.22$ nm. The error of the intensity due to the detection system was ± 0.5 units in a range of 0–255 units. The resulting error was around $d_{\text{cleft}} = \pm 0.15$ nm. The estimated errors of the parameters of the optical model are summarized in Table 1 together with the resulting errors
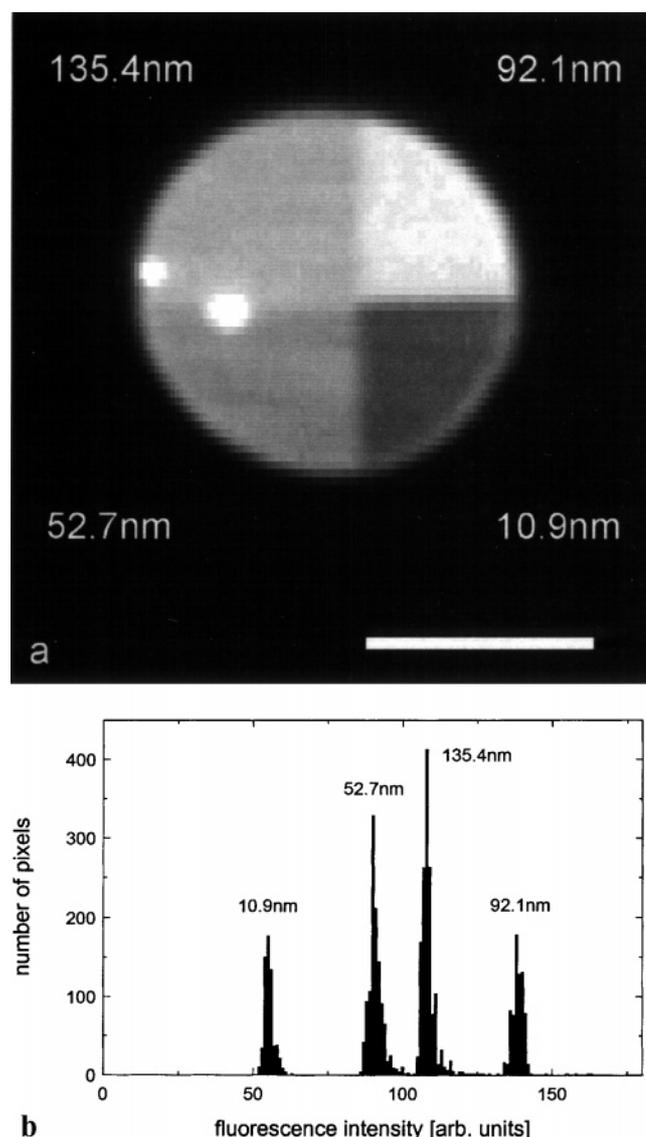

Fig. 7a,b. Fluorescence of a single ghost. **a** Image taken by a CCD-camera. The thickness of the four oxide layers is indicated. The scale bar is 5 µm. (The bright spots are dye crystals.) **b** Histogram of fluorescence intensity on the four regions. The number of pixels with a certain intensity is plotted versus the intensity in 8-bit resolution
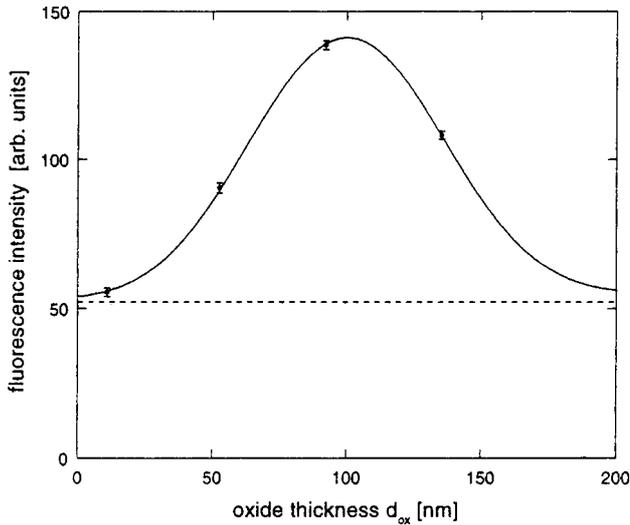
Fig. 8. Fluorescence intensity of a ghost stained with the dye DiIC$_{12}$ versus the thickness d_{ox} of silicon dioxide. The mean and $\pm\sigma$-values of the Gaussians are shown as obtained from the histograms of Fig. 7. The optical theory is fitted with a distance $d_{cleft} = 12.1$ nm (stochastic error ± 0.4 nm) between membrane and oxide. The dotted line marks the background

Δd_{cleft}. We obtained $\Delta d_{cleft} = \pm 0.77$ nm for the total systematic error.

The total error – stochastic and systematic – of a single measurement was $\Delta d_{cleft} = \pm 0.87$ nm.

2.3 Roughness

We estimated the inhomogeneity of adhesion from the width of the distributions of fluorescence intensity on regions with constant oxide thickness (Fig. 7). The theory of fluorescence interference (Fig. 8) indicates a change of intensity of 1.39 units per 1 nm oxide at $d_{ox} = 52.7$ nm. From $\sigma = 1.71$ we obtained a variation of $\Delta d_{cleft} = \pm 1.3$ nm the water layer between membrane and chip. At a thickness $\Delta d_{ox} = 135.4$ nm the slope is -1.47 units per 1 nm oxide. With $\sigma = 1.37$ we obtained a variation $\Delta d_{cleft} = \pm 1.0$ nm. These are upper limits of the roughness, as an inhomogeneity of illumination and the noise of the camera contribute to the variation of intensity, too.

Table 1. Parameters of the optical theory. The values in the second column are used in the computations. The third column presents the errors of the parameters. They are estimated on the basis of the pertinent literature and on the physics of the apparatus, respectively

Parameter	Value	Systematic error	Resulting error in d_{cleft}
n_{Si} at $\lambda = 633$ nm	3.87	± 0.05	± 0.00 nm
κ_{Si} at $\lambda = 633$ nm	0.017	± 0.005	∓ 0.04 nm
n_{cleft}	1.333	$+0.05$	-0.50 nm
n_{mem}	1.450	± 0.05	∓ 0.06 nm
d_{mem}	4.0 nm	± 0.5 nm	∓ 0.04 nm
n_{cyt}	1.333	$+0.05$	-0.02 nm
angle of transition dipole	90°	$-10°$	-0.03 nm
aperture $_{excitation}$	47.3°	$\pm 1°$	± 0.42 nm
aperture $_{emission}$	48.6°	$\pm 1°$	± 0.29 nm
max. of spectrum $_{emission}$	565 nm	5 nm	± 0.01 nm

2.4 Photobleaching

A problem with the fluorescence measurements is the selective photobleaching of the dye. The light intensity at the position of the membrane is not identical on the four steps of different height. As a consequence the rate of irreversible bleaching of the dye by photochemical reactions from the excited state is not identical. The relative intensity of fluorescence on the four steps may change. An example is shown in Fig. 9 when a cell was observed for 40 ms before and after 10 s of illumination. The first data set led to a distance $d_{cleft} = 12.2 \pm 0.3$ nm (stochastic error). The relative intensities of the four data points were changed in the second measurement due to photobleaching. We obtained $d_{cleft} = 16.0 \pm 3.5$ nm. The quality of the fit was lower, as the condition of homogeneous staining was no longer fulfilled.

2.5 Cell population

We evaluated the fluorometric data of 25 ghosts. The mean distances d_{cleft} of the membrane from silicon dioxide with their total stochastic error are shown in Fig. 10. As an average of the distances weighted with their stochastic error
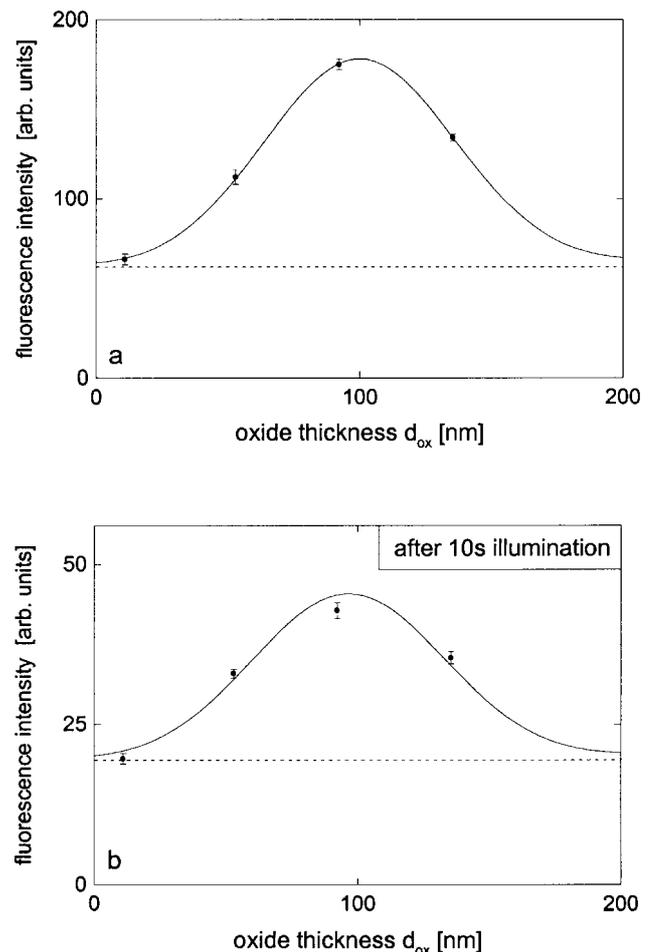

Fig. 9. Effect of photobleaching. Fluorescence intensity (mean and $\pm\sigma$-value) versus thickness d_{ox} of oxide without (upper figure) and with photobleaching (lower figure). The theory is fitted with a distance $d_{cleft} = 12.2$ nm (stochastic error ± 0.3 nm) without bleaching and with $d_{cleft} = 16.0$ nm (stochastic error ± 3.5 nm) after bleaching
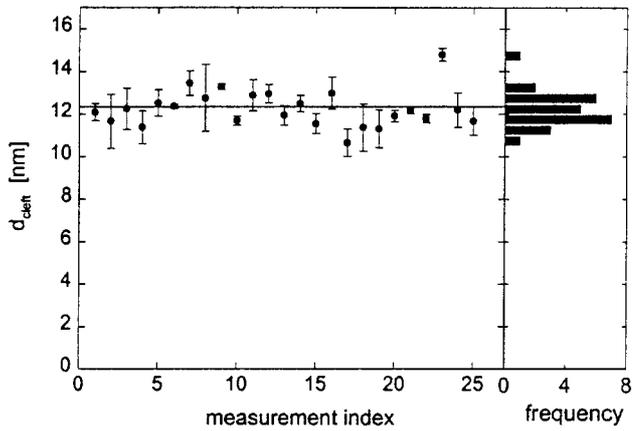
Fig. 10. Population of ghosts. Distance d_{cleft} between membrane and oxide of 25 freshly prepared ghosts. The bars indicate the stochastic error of a single measurement. The average distance is $d_{cleft} = 12.4 \pm 0.7$ nm

we obtained $d_{cleft} = 12.4$ nm. The standard deviation of the population was ± 0.7 nm. Modifications of the glycocalix by the preparation may give rise to a certain variation.

2.6 Glycocalix

The surface of erythrocytes is covered with a coat of negatively charged carbohydrates attached to proteins such as glycophorin A and band-3 protein [29]. The three-dimensional conformation of this glycocalix is unknown. A distance of $d_{cleft} = 12.4$ nm between the plane of lipid headgroups in the membrane and the substrate of silicon dioxide is compatible with a folded glycocalix on the positively charged polyelectrolyte poly-lysine. Note that the value of 12.4 nm was obtained with the refractive index of water (Table 1). If the actual refractive index in the cleft is larger due to protein, the thickness is reduced accordingly. The adhesion of erythrocytes to surfaces with and without poly-lysine was investigated extensively with RIC- microscopy and other techniques [30, 36–38]. However, no value for the distance between membrane and substrate was given in these studies. An average thickness of the glycocalix of 5.9 nm was estimated from binding of small gold particles as seen by electronmicroscopy [39].

2.7 Upper membrane

The fluorescence pattern of the attached membrane was superposed by circular fringes in some cells (Fig. 5). We assign this effect to the upper membrane. If the attached cell has the shape of a flat cupola, the upper membrane is in the focus of the microscope. Then the interference rings, which appear when the membrane crosses several maxima of the standing waves of the electromagnetic field, are not blurred.

An example is shown in Fig. 11a. We counted the maxima of interference along a cross-section and compared them with their position in the optical model as shown in Fig. 11c. As a result we obtained a set of distances of the upper membrane as plotted in Fig. 11b.

An attached cell has the shape of a spherical cap when the bending energy of the membrane equilibrates with the adhesion energy for strong adhesion [40]. We fitted the data of Fig. 11b by a circle of radius $R = 13\,\mu m$ with a height $h = 1.1\,\mu m$ of the cap. The radius of the attached region $a = 5\,\mu m$ and the contact angle $\Psi_{eff} = 24°$ follow from the stereometric relations of a spherical cap. The total area A of the membrane and the volume V of the cap are

$$A = \pi(4Rh - h^2), \quad V = \frac{\pi h^2}{3}(3R - h).\qquad(5)$$
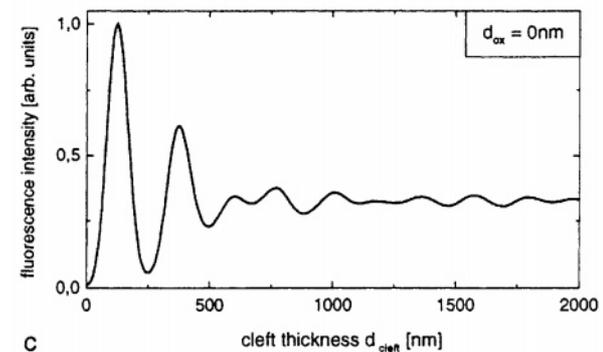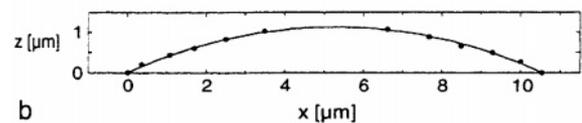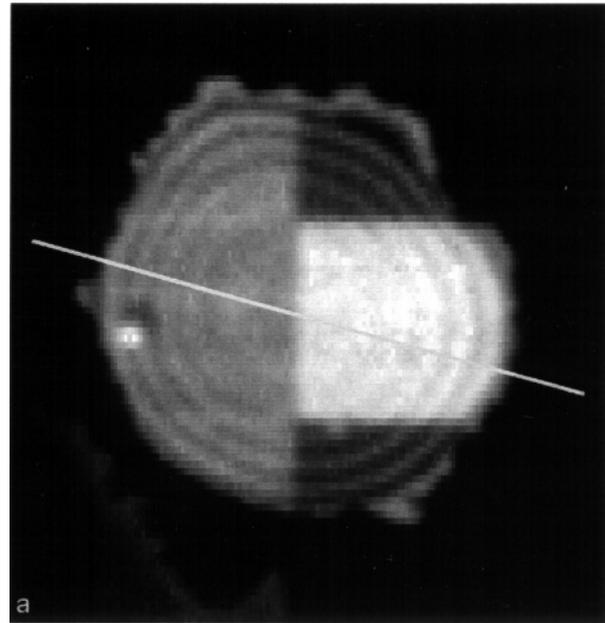

Fig. 11a–c. Fluorescence of a ghost with fringes. **a** Image taken with a CCD camera. The white line marks the position of the profile. **b** Profile of the upper membrane. The dots are obtained by counting the bright rings of intensity and comparing them with the optical theory. The data are fitted with a circle of radius $R = 13\,\mu m$ with a height $h = 1.1\,\mu m$ of the cap. **c** Theoretical fluorescence intensity as a function of the distance of a membrane from the silicon in water

We obtained $A \approx 175\,\mu m^2$ and $V \approx 48\,\mu m^3$. The volume of a sphere enclosed by the membrane would be $V_0 \approx 220\,\mu m^3$ (radius $R_0 \approx 3.7\,\mu m$). The origin of the considerable reduction of the volume is not known. It may be due to transient damage of the cell during the process of adhesion.

3 Conclusions

The present paper shows that FLIC-microscopy is an adequate technique to investigate cell adhesion on silicon. It combines the advantages of the two established methods of RIC-microscopy and TIRF-microscopy – the precision of an interference technique and the specific labelling of the membrane by a fluorescent dye. The result with respect to the distance between membrane and support is superior to the data obtained with the established methods. The novel technique may be developed further to measure distance maps at microscopic resolutions and to observe the dynamics of fluctuations. Applications to nerve cells and lipid membranes may be envisaged.

References

1. P. Fromherz: Ber. Bunsenges. Phys. Chem. **100**, 1093 (1996)
2. P. Fromherz, A. Offenhäusser, T. Vetter, J. Weis: Science **252**, 1290 (1991)
3. P. Fromherz, A. Stett: Phys. Rev. Lett. **75**, 1670 (1995)
4. R. Weis, P. Fromherz: Phys. Rev. E **55**, 877 (1997)
5. A.S.G. Curtis: J. Cell Biol. **20**, 199 (1964)
6. C.S. Izzard, L.R. Lochner: J. Cell. Sci. **21**, 129 (1976)
7. D. Gingell, I. Todd: Biophys. J. **26**, 507 (1979)
8. H. Verschueren: J. Cell Sci. **75**, 279 (1985)
9. M. Schindl, E. Wallraff, B. Deubzer, W. Wilke, G. Gerisch, E. Sackmann: Biophys. J. **68**, 1177 (1995)
10. D. Axelrod: J. Cell. Biol. **89**, 141 (1981)
11. D. Axelrod, N.L. Thompson, T.P. Burghardt: J. Microsc. **129**, 19 (1983)
12. D. Gingell, I. Todd, J. Bailey: J. Cell Biol. **100**, 1334 (1985)
13. I. Todd, J.S. Mellor, D. Gingell: J. Cell Sci. **89**, 107 (1988)
14. W.M. Reichert, G.A. Truskey: J. Cell Sci. **96**, 219 (1990)
15. J.D. Burmester, G.A. Truskey, W.M. Reichert: J. Microsc. **173**, 39 (1994)
16. A. Lambacher, P. Fromherz: Appl. Phys. A **63**, 207 (1996)
17. O. Wiener: Wied. Ann. 40, 203 (1890)
18. H. Kuhn: in Techniques of Organic Chemistry, Vol.1, part IIIB. Eds. A. Weissberger, B.W. Rossiter (Wiley, New York, 1972) p. 577
19. K.H. Drexhage: Progr. Optics **12**, 163 (1974)
20. G. Schwoch, H. Passow: Mol. Cell. Biochem. **2**, 197 (1973)
21. J. Sondermann: Justus Liebigs Ann. Chem. **749**, 183 (1971)
22. P. Fromherz: Chem. Phys. Lett. **26**, 221 (1974)
23. P.J. Sims, A.S. Waggoner, C.H. Wang, J.F. Hoffman: Biochemistry **13**, 3315 (1974)
24. D. Axelrod: Biophys.J. **26**, 557 (1979)
25. D.E. Wolf: Biochemistry **24**, 582 (1985)
26. D.M. Benson, J. Bryan, A.L. Plant, A.M. Gotto, L.C. Smith: J. Cell Biol. **100**, 1309 (1985)
27. S. Wolf, R.N. Tauber: Silicon Processing for the VLSI Era. Vo.1, (Lattice Press, Sunset Beach, CA, 1986)
28. P. Fromherz, G. Reinbold: Thin Solid Films **160**, 347 (1988)
29. J. Viitala, J. Järnefelt: Trends Biochem. Sci. **10**, 392 (1985)
30. N.E. Thomas, W.T. Coakley, C. Winters: Coll. Surf. B **6**, 139 (1996)
31. A. Lambacher, P. Fromherz: in preparation
32. M. Born, E. Wolf: Principles of Optics. (Pergamon, Oxford, 1980)
33. G.E. Jellison, F.A. Modine: Optical constants for silicon detected by ellipsometry (Oakridge National Laboratory, 1982)
34. Landolt-Börnstein: 6th Edition, vol. II, part 8 (Springer, Berlin, 1962)
35. W.H. Press, B.P. Flannery, S.A. Teukolsky, W.T. Vetterling: Numerical Recipes in C. (Cambridge University Press, Cambridge 1988)
36. D. Gingell, I. Todd: J. Cell Sci. **41**, 135 (1980)
37. H. Wolf, D. Gingell: J. Cell Sci. **63**, 101 (1983)
38. E. Donath, D. Gingell: J. Cell Sci. **63**, 113 (1983)
39. W. Linss, C. Pilgrim, H. Feuerstein: Acta Histochem. **91**, 101 (1991)
40. U. Seifert, R. Lipowsky: Phys. Rev. A **42**, 4768 (1990)